Seismic Resolution Enhancement by Frequency-Dependent Wavelet Scaling

Shuangquan Chen and Yanghua Wang

***Abstract*— When seismic waves propagate through the earth, their high-frequency energy is absorbed by subsurface viscoelastic media. Seismic wavelet appears to be stretched out, as it is dominated by low-frequency components. In order to enhance seismic resolution, we propose here a wavelet compression method that utilizes the scale characteristic in the Fourier transform. The novelty of the scheme is a frequency-dependent scaling that extends the amplitude spectrum to both high- and low-frequency axes simultaneously. This is for the first time to make this frequency-dependent proposal, instead of a constant scaling scheme in the classic Fourier theory. It compresses seismic wavelet in the time domain and also simplifies the wavelet form effectively. This frequency-dependent scaling scheme leads to a transferring filter that is applicable to seismic field data. It results in an improvement in data resolution and in the ability of thin-layer identification, which will facilitate further seismic inversion and reservoir characterization.**

***Index Terms*— Resolution enhancement, seismic data processing, signal processing.**

I. Introduction

THIS letter presents a wavelet scaling scheme for enhancing seismic resolution. Seismic wavelet controls seismic resolution. The shorter the wavelet breadth, the higher will be the seismic resolution, and vice versa.

When seismic waves propagate through the subsurface media, the wavelet is broadened gradually along the ray paths because of the accumulated absorption effect. Seismic reflection profiles appear to be dominated by low frequencies. An objective for geophysics is to improve seismic resolution, for being capable to characterize thin-layered hydrocarbon reservoirs. Seismic data processing methods for recovering high-frequency components include predictive deconvolution, Gabor deconvolution, and inverse Q-filtering.

Manuscript received October 9, 2017; revised November 23, 2017 and February 8, 2018; accepted February 20, 2018. This work was supported in part by the National Natural Science Foundation of China under Grant 41574108, in part by the Science Foundation of China University of Petroleum-Beijing under Grant 2462015YQ0503, and in part by the Open Project Program of Sinopec Key Laboratory of Multicomponent Seismic Technology. *(Corresponding author: Shuangquan Chen.)*

S. Chen is with the State Key Laboratory of Petroleum Resources and Prospecting, China University of Petroleum, Beijing 102249, China, and also with the CNPC Key Laboratory of Geophysical Prospecting, China University of Petroleum, Beijing 102249, China (e-mail: chen.shuangquan@hotmail.com).

Y. Wang is with the Centre for Reservoir Geophysics, Department of Earth Science and Engineering, Imperial College London, London SW7 2BP, U.K. (e-mail: yanghua.wang@imperial.ac.uk).

Color versions of one or more of the figures in this letter are available online at http://ieeexplore.ieee.org.

Digital Object Identifier 10.1109/LGRS.2018.2809564

Deconvolution [1], [2] as an essential part of seismic data processing has developed in a series of aspects. Wiener filters were derived from the theory of Robinson deconvolution [1], [3], and solidified and extended in [4] and [5]. The algorithms rest on a convolutional model that a seismic trace is a reflectivity series convolved with a seismic wavelet. Various techniques include deconvolution considering stationary seismic wavelet [6]–[8], deconvolution with a mixed-phase wavelet [9], time-varying Wiener filtering to handle nonstationary seismic data [10], Gabor deconvolution to enhance seismic resolution [11]–[13], and multichannel blind deconvolution, which exploits the lateral coherence among the seismic traces [14]–[16].

Seismic resolution can also be enhanced by inverse Q-filtering, compensating for the attenuation induced to seismic waveforms. Conventionally, the inverse Q-filter was for the correcting phase only [17], [18] and did not alter high-frequency amplitudes. Wang [19]–[21] proposed stable inverse Q-filters that compensate for seismic amplitudes and correct the phases simultaneously.

Theoretically, the scale characteristic of Fourier transform can also be exploited to improve seismic resolution. For a seismic wavelet $w(t)$, where t is time, its Fourier spectrum $W(f)$ can be written as $W(f) = |W(f)|e^{i\varphi(f)}$, where f is the frequency, $|W(f)|$ is the amplitude spectrum, and $\phi(f)$ is the phase spectrum. According to Fourier theory [22], when seismic wavelet $w(t)w(t)$ is compressed by a scaling factor $a > 1$, the corresponding $W(f)W(f)$ will be changed accordingly

$$w(at) \leftrightarrow \frac{1}{a}\left|W\left(\frac{f}{a}\right)\right| e^{i\phi(f/a)}. \tag{1}$$

For $a > 1$, the amplitude spectrum will be shifted to a higher frequency band [23] and, hence, seismic resolution increases. If the wavelet is stretched by a scale factor $0 < a < 10 < a < 1$, the amplitude spectrum will be shifted to a lower frequency band, and seismic resolution decreases.

Fig. 1(a) displays a Berlage minimum-phase wavelet, defined with a peak frequency of 30 Hz. Fig. 1(b) shows that the original 30-Hz wavelet is compressed by a factor of 2 and is equivalent to a 60-Hz wavelet. The compressed wavelet shown in Fig. 1(c) has a wide frequency band and a high peak frequency. However, it is also observed from Fig. 1(c) that the normalized amplitudes at low frequencies between 0 and 25 Hz are weaker than those before wavelet compression, as the spectrum is shifted toward the high-frequency axis. How to maintain and even improve those amplitudes of

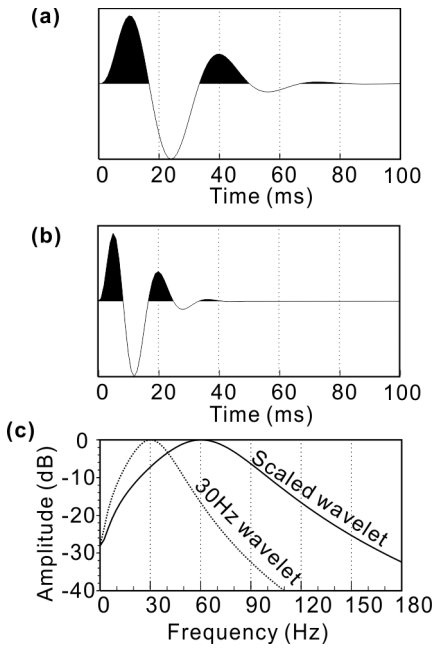

Fig. 1. Wavelet compression using a constant scaling factor. (a) Berlage wavelet with a peak frequency of 30 Hz. (b) Wavelet is compressed by a factor of 2. Compressed 30-Hz wavelet is equivalent to a 60-Hz wavelet. (c) Amplitude spectra of these two wavelets.

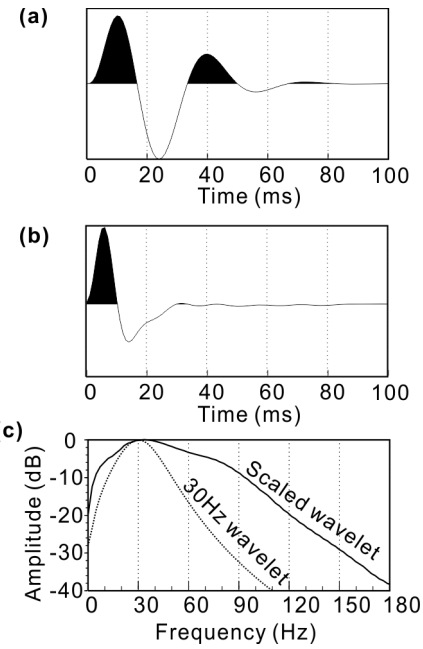

Fig. 2. Wavelet compression using a frequency-dependent scaling factor. (a) 30-Hz Berlage wavelet, same as that shown in Fig. 1(a). (b) Compressed wavelet, using a frequency-dependent scaling factor. (c) Amplitude spectra of these two wavelets.

low-frequency components is an objective of this letter. We propose here a frequency-dependent wavelet scaling method so as to compress seismic wavelet and to improve the resolution. When applying this method to seismic data with a thin-layered sandstone reservoir, we will see that the filtered seismic profile has detailed information about the thin-layered sand body and clearer fault displays, which will be confirmed by well-tie analyses.

II. Methodology

A. Theory

In order to compress seismic wavelets by stretching the frequency spectra, and all the more while increasing the amplitudes of low frequencies. We propose to modify (1), by introducing a frequency-dependent scaling factor

$$a(f) = \begin{cases} \dfrac{f_r + f}{2f_r}, & 0 \le f < f_r \\ \dfrac{(n-2)f_r + f}{(n-1)f_r}, & f_r \le f < nf_r \\ 2, & f \ge nf_r \end{cases} \tag{2}$$

where f_r is a reference frequency and $n \ge 5$ is an adjustable integer. When applying this scaling factor $a(f)$ to the frequency spectrum

$$\left| W\left(\frac{f}{a(f)}\right)\right| \exp\left(i\phi\left(\frac{f}{a(f)}\right)\right) \tag{3}$$

the spectrum will be stretched toward both high- and low-frequency axes. For frequencies decreasing from f_r to 0 Hz, the scaling factor is reduced from 1 to 0.5, and the spectrum is stretched to the left. For frequencies between f_r and nf_r, the scaling factor is increased from 1 to 2, and the spectrum is stretched to the right. For frequencies $f \ge nf_r$, the scaling factor is fixed to be 2, and the spectrum is stretched to the right.

We set reference frequency $f_r$to be a half of peak frequency f_p, and $n = 5$ in this letter. A Ricker wavelet for instance has the frequency bands: 0.482 f_p and 1.637 f_p [24], [25], and the highest effective frequency is about $2.5f_p$. Therefore, reference frequency f_r presents roughly the left boundary of the frequency band, and nf_r with $n = 5$ covers the highest effective frequency.

B. Effectiveness

Let us demonstrate the effectiveness of this frequency-dependent scaling scheme using the same wavelet as in Fig. 1(a). A compressed wavelet is shown in Fig. 2(b) and has a much simpler form. This is because the scheme not only expands to the high frequencies but also stretches to the low frequencies [Fig. 2(c)]. Seismic resolution improvement depends upon the improvement of two parameters: the bandwidth and the central frequency [26]. Fig. 2 clearly indicates a good improvement on those parameters, and in turn ON the seismic resolution.

A synthetic wedge model, shown in Fig. 3(a), represents a sandstone embedded in a shale background. This is generated using the Berlage wavelet that has a peak frequency of 30 Hz. Wavelet compression using a constant factor of 2 produces a wavelet-compressed section of Fig. 3(b), which is equivalent to a synthetic section when using the Berlage wavelet of 60-Hz peak frequency. In seismic interpretation, a quarter of the dominant wavelength (λ) is generally used to evaluate the resolution by the composited maximum amplitude.

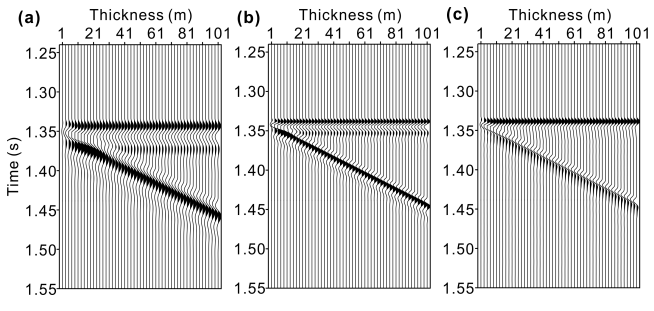

Fig. 3. Synthetic wedge section. (a) Synthetic section, generated using the Berlage wavelet with a 30-Hz peak frequency. (b) Wavelet-compressed section, using a constant scaling factor of 2. (c) Wavelet-compressed section, using a frequency-dependent scaling factor.

The velocity of sandstone in the wedge model is set to be $V = 2000$ m/s, and thus the resolution ability of the 30-Hz wavelet is $V/4f \approx 17$ m. The composited maximum amplitude of the synthetic seismic section is about 34 m, as shown in Fig. 3(a). Accordingly, the resolution ability of the 60-Hz wavelet is about 8.5 m, and the composited maximum amplitude of the synthetic seismic section is about 17 m, as shown in Fig. 3(b).

However, using the frequency-dependent scaling factor, the compressed wavelet [Fig. 2(b)] has a much simpler form, because of the spectral expansion of low frequencies. It leads to a high-resolution seismic section, as shown in Fig. 3(c), which clearly indicates that the resolution ability of the 60-Hz wavelet is closer to 8.5 m, rather than the composited maximum amplitude at 17 m, in the previous case.

C. Signal Processing Workflow

For processing seismic data, we establish a workflow which consists of three steps: wavelet estimation from the entire field seismic data set, filter construction based on scaled wavelet, and application to the seismic data set.

A seismic trace $s(t)$ can be expressed as the convolution between seismic wavelet $w(t)$ and reflectivity series $r(t)$. This convolution model in the frequency domain can be written as

$$S(f) = W(f)R(f). \tag{4}$$

If the wavelet is scaled, the transferred seismic trace can be written as follows:

$$\hat{S}(f) = \hat{W}(f)R(f) \tag{5}$$

where $\hat{W}(f)$ is the stretched spectrum, which has a time-domain wavelet $\hat{w}(t)$. Therefore, we have an equation

$$\hat{S}(f) = \frac{\hat{W}(f)}{W(f)}S(f) = H(f)S(f) \tag{6}$$

where $H(f)$ is a transferring filter that can be obtained through the wavelet scaling

$$W(f)H(f) = \hat{W}(f) \tag{7}$$

where W is the spectrum of the estimated wavelet and $\hat{W}$ represents the stretched spectrum.

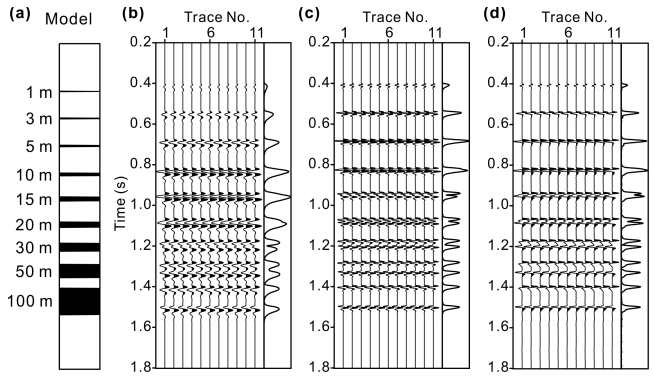

Fig. 4. Interbed thin-layer model. (a) Sketch of the thin-layer model, composed of sandstone layers with different thicknesses. (b) Synthetic seismic trace of a 30-Hz Berlage wavelet. (c) Scaled seismic trace, using a constant scaling factor of 2. (d) Wavelet-compressed seismic trace, using a frequency-dependent scaling factor, scaled from (b). The amplitude envelopes are displayed on the right-hand side of each individual trace panel.

Based on (7), we construct the transferring filter $H(f)$ in a least-squares sense

$$H = (\bar{W}W + \sigma^2)^{-1}\bar{W}\hat{W} \tag{8}$$

where $\bar{W}(f)$ is the complex conjugate of $W(f)$ and σ^2 is a small positive factor for stabilizing the least-squares solution.

According to (6), we can apply this filter to seismic data, producing seismic data $\hat{s}(t)$ with improved resolution. However, (8) indicates that this filter is amplitude dependent, since the stabilization procedure will damp the frequency components, likely the high frequencies, with a small amplitude. We set the value of the factor σ^2 to be 0.001 of the maximum energy (amplitude squared) for the synthetic examples and for the field data applications in this letter.

In summary, the workflow should include the following three steps:

1) estimating a seismic wavelet $w(t)$ from the input seismic data set [27];
2) stretching frequency spectrum from $W(f)$ to $\hat{W}(f)$, using frequency-dependent scaling factor $a(f)$, and calculating the transferring filter $H(f)$ based on the spectra $W(f)$ and $\hat{W}(f)$;
3) processing the entire seismic data set using the single transferring filter $H(f)$.

We demonstrate this workflow using an interbedded-layer model with nine sandstone layers [Fig. 4(a)]. The background layer is shale with a constant velocity. Nine high-velocity sandstone layers have thicknesses of 1, 3, 5, 10, 15, 20, 30, 50, and 100 m, sequentially, from the top to the bottom. The velocity is also 2000 m/s. Fig. 4(b) shows the synthetic seismic record, created by convoluting the model with a Berlage wavelet of 30-Hz peak frequency, the same as the wedge model example.

Fig. 4(c) shows the wavelet-compressed result by applying a constant scaling factor $a = 2$. The peak frequency has migrated from 30 to 60 Hz. Fig. 4(d) shows the result of applying the frequency-dependent scaling factor, to the seismic profile of Fig. 4(b).

For the sake of convenience in identifying reflections in the seismic record, we duplicate 21 traces displayed

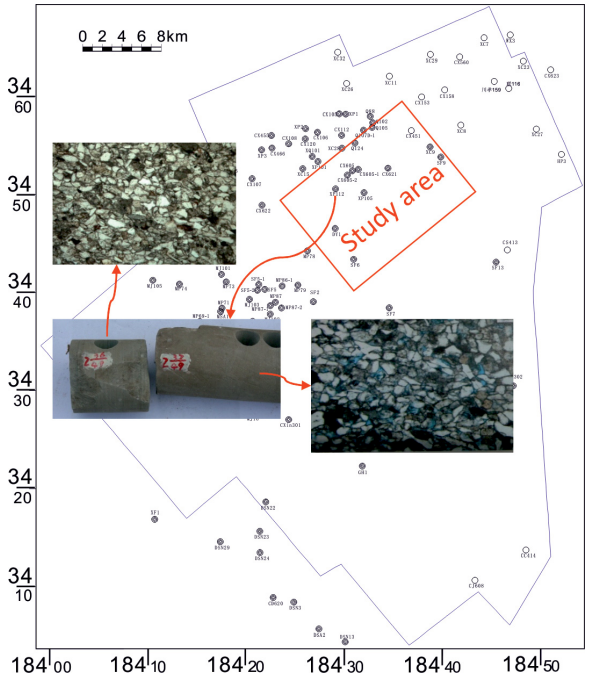

Fig. 5. Location map of the study area for seismic resolution enhancement. Inset: one well core and two microscope slices that indicate a tight sand reservoir.

in Fig. 4(b)–(d). For the three seismic records, we calculate the amplitude envelope curves, which are displayed at the right-hand side of each individual seismic panel. Comparison of the amplitude envelope curves also verifies that the resolution is improved by the wavelet scaling process, and that the ability of the thin-layer identification is enhanced.

III. Application to Seismic Data

Here we apply the wavelet scaling scheme to a land seismic data set from the western Sichuan basin, China [28]. In this study area (Fig. 5), the resolution of seismic records received from the target horizon is relatively low, as the seismic section has a dominant frequency of about 20 Hz. Thus, seismic resolution enhancement is a very important processing step for the consequent inversion and interpretation works. The target hydrocarbon reservoir consists of thin layers and tight sands. One of the well cores is also displayed in Fig. 5, and two core microscope slices indicate that the reservoir is tight sand.

The data set is a processed seismic profile [Fig. 6(a)] through conventional processing modules, including prestack time migration, noise attenuation, and wavelet zero-phasing. After the wavelet compression processing [Fig. 6(b)], the inter-layered sandstone reservoir is clearly revealed. The signal-to-noise ratio of the seismic section before and after the scale processing is 6.14 and 6.06, respectively. It is maintained at a similar level.

In particular, for the main target at time $t = 2.5$ s, the zoomed-in comparison of seismic sections is shown in Fig. 7, in which an event in the thin-layer sandstone (indicated by arrows), together with one of the small faults (indicated by an ellipse), can be seen clearly.

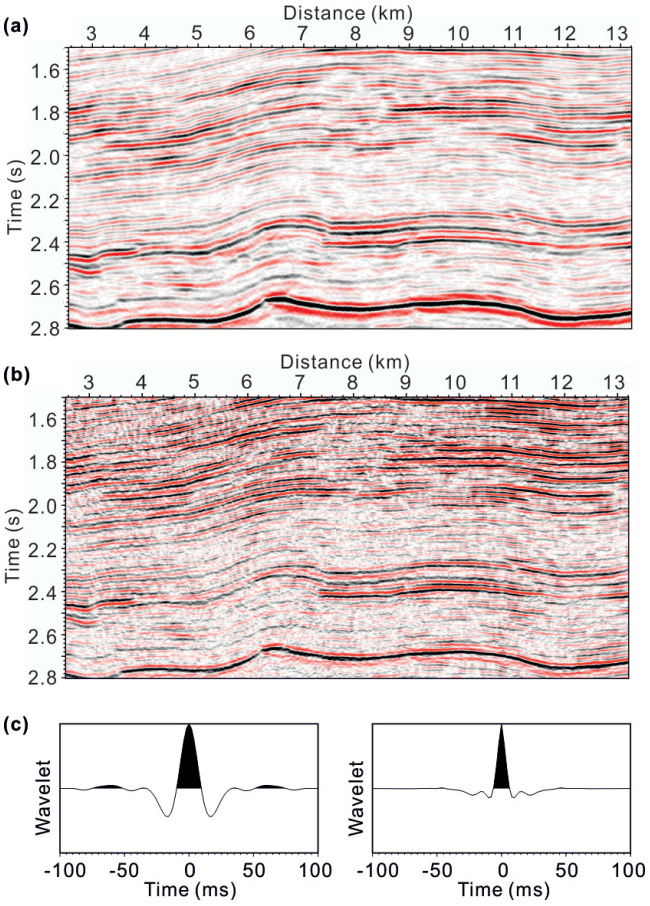

Fig. 6. (a) Field seismic section before wavelet scale processing. (b) Seismic section after wavelet scale processing. (c) Two wavelets estimated from sections (a) and (b), respectively.

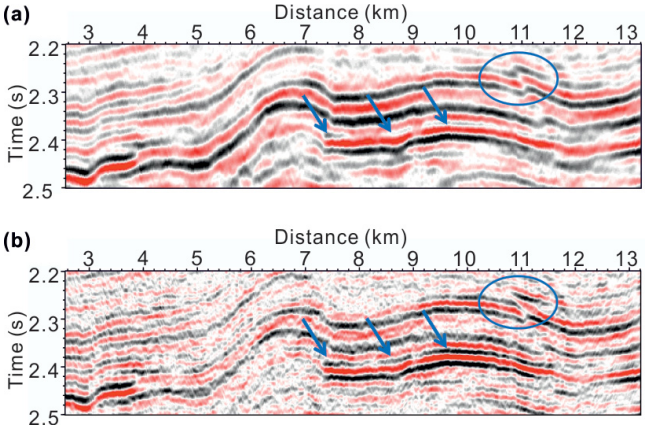

Fig. 7. Zoomed-in display corresponding to the time window between 2.2 and 2.5 s in Fig. 6. (a) Before the wavelet transfer processing. (b) After the wavelet transfer processing. After the resolution enhancement, more thin-layer information (arrows) and a clearer fault (an ellipse) are displayed.

Fig. 8 shows a comparison of the well-to-seismic calibrations before and after wavelet scale processing. Fig. 8(a) shows density, P-wave velocity, and P- to S-wave velocity ratio (V_p/V_s) at the well location. The V_p/V_s curve indicates that there is a set of low-velocity thin-layer sandstones (red boxes in Fig. 8), interbedded with shale layers.

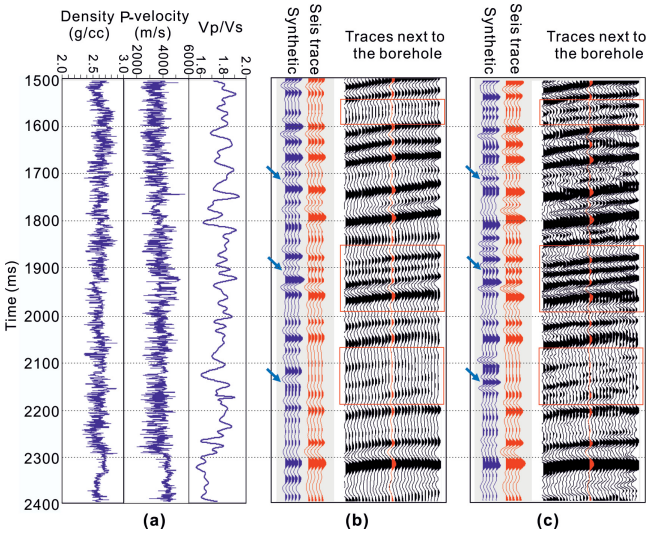

Fig. 8. (a) Well logs of density, the P-wave velocity, and the Vp/Vs ratio. (b) Comparison of the synthetic trace and the field seismic trace before the wavelet transfer processing. (c) Comparison of the synthetic trace and the field seismic trace after the wavelet transfer processing. Each of the synthetic and real seismic traces is plotted five times. The frame and arrows indicate some details of thin layers in the comparison.

Fig. 8(b) shows the synthetic and field seismic traces at the well location, before wavelet transfer processing. The synthetic trace is generated by the convolution between the reflectivity series, calculated from well logging, and a wavelet extracted from the seismic trace. A composite reflection wave appears (within the red rectangle) on both the synthetic trace and the field seismic trace at the well location.

Fig. 8(c) shows the result after resolution enhancement processing. Clearer thin-layer information is obtained from the wavelet-scaled section, as indicated by the arrows. A high correlation between the synthetic trace and the field seismic trace further verifies that these reflections revealed in wavelet-scaled sections are reliable reflections that were generated from interbedded low-velocity shales and thin sandstones.

IV. Conclusion

We have proposed a novel resolution enhancement technology by compressing seismic wavelets. When seismic wavelets are compressed, the dominant frequency increases, and the frequency bandwidth expands. Wavelet scaling factor is frequency dependent, and the scaled wavelet has a simple form. Therefore, we have had more of an ability to identify thin layers clearly from a reflection seismic profile. When we apply the wavelet-scaled seismic data to seismic inversion, we will be able to generate a high-resolution image for sand-body characterization.

Acknowledgment

The authors would like to thank the editor A. Frery for coordinating the review of this paper and approving it for publication.

References

[1] E. A. Robinson, "Predictive decomposition of seismic traces," *Geophysics*, vol. 22, no. 4, pp. 767–778, Oct. 1957.
[2] E. A. Robinson, "Predictive decomposition of time series with application to seismic exploration," *Geophysics*, vol. 32, no. 3, pp. 418–484, Jun. 1967.
[3] A. V. Oppenheim, "Superposition in a class of nonlinear systems," MIT Res. Lab. Electron., Cambridge, MA, USA, Tech. Rep. 432, 1965.
[4] E. A. Robinson and S. Treitel, "Principles of digital Wiener filtering," *Geophys. Prospecting*, vol. 15, no. 3, pp. 311–332, Sep. 1967.
[5] K. L. Peacock and S. Treitel, "Predictive deconvolution: Theory and practice," *Geophysics*, vol. 34, no. 2, pp. 155–169, Apr. 1969.
[6] D. W. Oldenburg, S. Levy, and K. P. Whittall, "Wavelet estimation and deconvolution," *Geophysics*, vol. 46, no. 11, pp. 1528–1542, Nov. 1981.
[7] S. Levy and D. W. Oldenburg, "Automatic phase correction of common-midpoint stacked data," *Geophysics*, vol. 52, no. 1, pp. 51–59, Jan. 1987.
[8] J. Longbottom, A. T. Walden, and R. E. White, "Principles and application of maximum kurtosis phase estimation," *Geophys. Prospecting*, vol. 36, no. 2, pp. 115–138, Feb. 1988.
[9] M. J. Porsani and B. Ursin, "Mixed-phase deconvolution," *Geophysics*, vol. 63, no. 2, pp. 637–647, Mar. 1998.
[10] M. van der Baan, "Time-varying wavelet estimation and deconvolution by kurtosis maximization," *Geophysics*, vol. 73, no. 2, pp. V11–V18, Mar. 2008.
[11] G. F. Margrave, P. C. Gibson, J. P. Grossman, D. C. Henley, V. Iliescu, and M. P. Lamoureux, "The Gabor transform, pseudodifferential operators, and seismic deconvolution," *Integr. Comput.-Aided Eng.*, vol. 12, no. 1, pp. 43–55, Jan. 2005.
[12] G. F. Margrave, M. P. Lamoureux, and D. C. Henley, "Gabor deconvolution: Estimating reflectivity by nonstationary deconvolution of seismic data," *Geophysics*, vol. 76, no. 3, pp. W15–W30, May 2011.
[13] Z. Chen, Y. Wang, X. Chen, and J. Li, "High-resolution seismic processing by Gabor deconvolution," *J. Geophys. Eng.*, vol. 10, no. 6, Oct. 2013, Art. no. 065002.
[14] N. Kazemi and M. Sacchi, "Sparse multichannel blind deconvolution," *Geophysics*, vol. 79, no. 5, pp. V143–V152, Sep. 2014.
[15] K. Nose-Filho, A. K. Takahata, R. Lopes, and J. M. Romano, "A fast algorithm for sparse multichannel blind deconvolution," *Geophysics*, vol. 81, no. 1, pp. V7–V16, Jan. 2016.
[16] R. Wang and Y. Wang, "Multichannel algorithms for seismic reflectivity inversion," *J. Geophys. Eng.*, vol. 14, no. 1, pp. 41–50, Jan. 2017.
[17] S. H. Bickel and R. R. Natarajan, "Plane-wave Q deconvolution," *Geophysics*, vol. 50, no. 9, pp. 1426–1439, Sep. 1985.
[18] N. D. Hargreaves and A. J. Calvert, "Inverse Q filtering by Fourier transform," *Geophysics*, vol. 56, no. 4, pp. 519–527, Apr. 1991.
[19] Y. Wang, "A stable and efficient approach of inverse Q filtering," *Geophysics*, vol. 67, no. 2, pp. 657–663, Mar. 2002.
[20] Y. Wang, "Inverse Q-filter for seismic resolution enhancement," *Geophysics*, vol. 71, no. 3, pp. V51–V60, May 2006.
[21] Y. Wang, *Seismic Inverse Q Filtering*. Oxford, U.K.: Blackwell, 2008.
[22] C. M. Rader, "Discrete Fourier transforms when the number of data samples is prime," *Proc. IEEE*, vol. 56, no. 6, pp. 1107–1108, Jun. 1968.
[23] R. Bansal and M. Matheney, "Wavelet distortion correction due to domain conversion," *Geophysics*, vol. 75, no. 6, pp. V77–V87, Nov. 2010.
[24] Y. Wang, "Frequencies of the Ricker wavelet," *Geophysics*, vol. 80, no. 2, pp. A31–A37, Mar. 2015.
[25] Y. Wang, "The Ricker wavelet and the Lambert W function," *Geophys. J. Int.*, vol. 200, no. 1, pp. 111–115, Jan. 2015.
[26] B. Z. Zhou, I. M. Mason, and P. J. Hatherly, "Tuning seismic resolution by heterodyning," *J. Geophys. Eng.*, vol. 4, no. 2, pp. 214–223, Apr. 2007.
[27] Y. Wang, "Generalized seismic wavelets," *Geophys. J. Int.*, vol. 203, no. 2, pp. 1172–1178, Nov. 2015.
[28] Q. Gan, D. Xu, J. Tang, and Y. Wang, "Seismic resolution enhancement for tight-sand gas reservoir characterization," *J. Geophys. Eng.*, vol. 6, no. 1, pp. 21–28, Jan. 2009.